Preparation and Characterization of Acetylated Nanocrystalline Cellulose-reinforced Polylactide Highly Regular Porous Films

Mingcong Xu,[a] Rue Yang,[b] Qiongtao Huang,[b] Xin Zhao,[c] Chunhui Ma,[a] Wei Li,[a,b,*] Jian Li,[a] and Shouxin Liu [a,*]

Nanocrystalline cellulose was prepared from bleached softwood kraft pulp using acid hydrolysis. Acetylated nanocellulose (AcNCC) and polylactic acid (PLA) were mixed together at different proportions under certain humidity conditions using a miscible method to prepare highly regular porous AcNCC/PLA composite films. The composites were characterized using scanning electron microscopy, transmission electron microscopy, thermogravimetric analysis, and Fourier transform infrared spectroscopy. The PLA/Ac-NCC-4 showed a uniform pore diameter distribution with diameter of 1.0 μm to 5.0 μm. The mechanical properties and thermal stability of the PLA composites were improved with the addition of AcNCC. The pore structure was regular and well distributed. When the AcNCC loading was 4%, the tensile strength and Young's modulus of the composites were 2.07 and 2.41 times higher than that of the pure PLA, respectively. The composites also exhibited high visible light transmission.

Keywords: Nanocrystalline cellulose; Acetylation; Polylactic acid; Highly regular porous film

Contact information: a: Key laboratory of Bio-based Material Science and Technology of Ministry of Education, Northeast Forestry University, Hexing Road 26, Harbin 150040, P. R.; b: Post-Doctoral Research Center, Yihua Lifestyle Technology Co., Ltd., Shantou, 515834, P. R. China; c: Key Laboratory of Pulp and Paper Science & Technology of Ministry of Education/Shandong Province, Qilu University of Technology, Jinan, 250353, China;
** Corresponding authors: liwei19820927@126.com; liushouxin@126.com*

INTRODUCTION

Nanocrystalline cellulose (NCC) is the most common polymer material found in nature. The low manufacturing costs, good thermal stability, excellent mechanical properties, such as a large surface area and high modulus, and other advantages have resulted in increasing interest in this material in recent years (Habibi *et al*. 2010; Li *et al*. 2011, 2013a). The abundance of hydroxyl groups on the surface of NCC makes it hydrophilic and insoluble in organic solvents, which limits its application with enhanced organic polymers. The NCC surface can be modified to make it miscible in chloroform and other organic solvents, while retaining the original characteristics of the nanocellulose. This can improve its dispersibility in organic polymers and enhance its effects (Lin *et al*. 2011; Li *et al*. 2013b; Habibi 2014; Lam *et al*. 2017).

Polylactic acid (PLA) is a synthetic polymer with excellent biocompatibility and biodegradability. It is non-toxic, non-irritating, has a high strength, high plasticity, is easily processed, and can be decomposed easily by a variety of microorganisms, plants, and enzymes to ultimately form water and carbon dioxide (Nakagaito *et al*. 2009; Kowalczyk *et al*. 2011; Fortunati *et al*. 2012; Frone *et al*. 2013; Ghalia and Dahman 2017). Therefore, PLA is considered to be one of the most promising biodegradable polymer materials.

However, the shortcomings of PLA include brittleness, poor thermal stability, and a low crystallization rate, which limit its applications in practice. Modified NCC is used in the preparation of enhanced PLA composite films by enhancing the mechanical properties and thermal stability and mitigating the brittleness of PLA (Shi *et al*. 2012; Haafiz *et al*. 2013; Xie *et al*. 2014; Fortunati *et al*. 2014). The properties of PLA can be effectively improved by adding acetylated NCC (AcNCC) to its matrix to prepare enhanced PLA composite film materials (Bilbao-Sáinz *et al*. 2010; Pankaj *et al*. 2014; Robles *et al*. 2015).

Materials with an ordered porous structure are widely applied in the fields of biotechnology, tissue engineering, and efficient separation (Shimomura 1993). Under high humidity conditions, water vapor is condensed on the polymer surface because of solvent evaporation (Jenekhe and Chen 1999). Water droplets accumulate on the polymer surface because of the temperature gradient in the solution under the action of capillary flow and reflux, which then results in an ordered porous polymer film (Srinivasarao *et al*. 2001; Zhao *et al*. 2003). The ability to form stable droplets is the key to the formation of a regular pore structure in polymer films (Widawski *et al*. 1994).

In this study, NCC was first acetylated and modified. Then, different amounts of AcNCC and PLA were dissolved in a chloroform solution. The PLA composite films with a porous structure were prepared using a water-assisted method. The structure, mechanical properties, thermal stability, and transmittance of the PLA/AcNCC cellular porous composite films prepared using different ratios of AcNCC and PLA were analyzed.

EXPERIMENTAL

Methods

Preparation of the NCC

The bleached softwood kraft pulp (BSKP) (Mudanjiang Hengfeng Paper Co. Ltd., Mudanjang, China) was ground to a 40 mesh to 60 mesh size with a wood flour-grinding machine (JL064, Shanghai Jiading instrument Co. Ltd., Shanghai, China). Ten grams of wood powder were added to 64 wt.% of H_2SO_4 at 45 °C, and the mixture was then stirred for 0.5 h, after which the samples became a pale-yellow liquid. After acid hydrolysis, the suspension was diluted with 500 mL of distilled water to terminate the reaction. The excess acid was removed by centrifugation/washing at 8000 rpm, and this process was repeated five times until the pH value of the suspension was approximately 3 to 5. The suspension was added to a dialysis bag and was washed with distilled water dialysis for 15 d until the pH value of the suspension was constant. Finally, the suspension was concentrated and freeze-dried before further use.

Preparation of the AcNCC

To prepare the AcNCC, 2 g of NCC were added to an appropriate amount of glacial acetic acid and underwent swelling for 3 h. The swollen NCC was filtered through filter paper and placed in a reactor. Then, 10 mL of acetic anhydride and 16 mL of acetic acid were added, and the resulting mixture was heated to 45 °C. While the mixture was stirred, 0.8 mL of a 5 M sulfuric acid solution was added. The AcNCC was obtained after the reaction was performed for 0.5 h. Finally, the obtained AcNCC was freeze-dried before further use.

Preparation of the highly regular porous composite films

To prepare the highly regular porous composite films, 5 g of PLA and 50 mL of chloroform were added to a conical flask and the PLA was completely dissolved using magnetic stirring. The prepared AcNCC powder was added to the chloroform and ultrasonication was applied to the resulting mixture for 3 h to obtain a 2 wt.% solution. The PLA and PLA/AcNCC solutions were combined, the mixtures were degassed, and the PLA/AcNCC films were generated with a saturated NaCl solution (relative humidity = 75%) *via* the solution casting method. The AcNCC/PLA composites were prepared by adding AcNCC at mass fractions of 0%, 2%, 4%, 8%, and 12%, which were denoted as PLA, PLA/AcNCC-2, PLA/AcNCC-4, PLA/AcNCC-8, and PLA/AcNCC-12, respectively. After the solvent was volatilized, the resulting PLA films were dried at 50 °C for 1.5 h to remove the residual solvent and the films were placed in a desiccator in preparation for the experiments.

Characterization

Transmission electron microscopy (TEM) observations were made with a FEI/Philips Tecnai G2 (Philips, Eindhoven, The Netherlands) operated at 80 kV. A drop of diluted NCC suspension was deposited on 300 mesh screen carbon-coated grids (the drop size of the suspension was 2 mm in diameter) and allowed to dry at room temperature (25 °C). The sample was stained with phosphotungstic acid (2 wt.%) for 30 s.

Fourier transform infrared (FT-IR) spectra were measured using a Nicolet iS10 FT-IR instrument (Thermo Scientific, Waltham, USA). The spectra were measured in the attenuated total reflectance mode and the data was recorded over the range of 650 cm^{-1} to 4000 cm^{-1} with a resolution of 1 cm^{-1}.

Thermogravimetric analysis (TGA) was performed using a TGA-Q50 TG analyzer (TA, New Castle, DE, USA). The temperature programs for the dynamic tests were run over a temperature range of 25 °C to 600 °C at a heating rate of 10 °C/min.

Microstructural analysis was performed using scanning electron microscopy (SEM) (QUANTA 200, FEI, Hillsboro, OR, USA). The sample surfaces were coated with a thin layer of gold using a BAL-TEC SCD 005 sputter coater (Leica, Wetzlar, Germany) to provide electrical conductivity.

Mechanical properties of the PLA and PLA/AcNCC composite films were analyzed using an RGT-20A instrument (Shenzhen Reger Instrument, Shenzhen, China). To characterize each type of film, three samples were fabricated with a length of 100 mm ± 2 mm, width of 10 mm ± 0.3 mm, and thickness of 0.1 mm ± 0.05 mm. The optical transmittance was measured over the range of 300 nm to 800 nm using ultraviolet-visible spectroscopy.

RESULTS AND DISCUSSION

TEM Analysis

Figure 1 shows the TEM images and length distributions of the NCC and AcNCC. The NCC showed a rod-like structure with a rod diameter of 10 nm to 20 nm and length of 75 nm to 150 nm. Because of the acidic conditions of the acetylation modification, the prepared AcNCC maintained a rod-like structure with a diameter of 10 nm to 20 nm and decreased length of 45 nm to 100 nm. Moreover, the length distribution of the AcNCC was more uniform than that of the NCC.

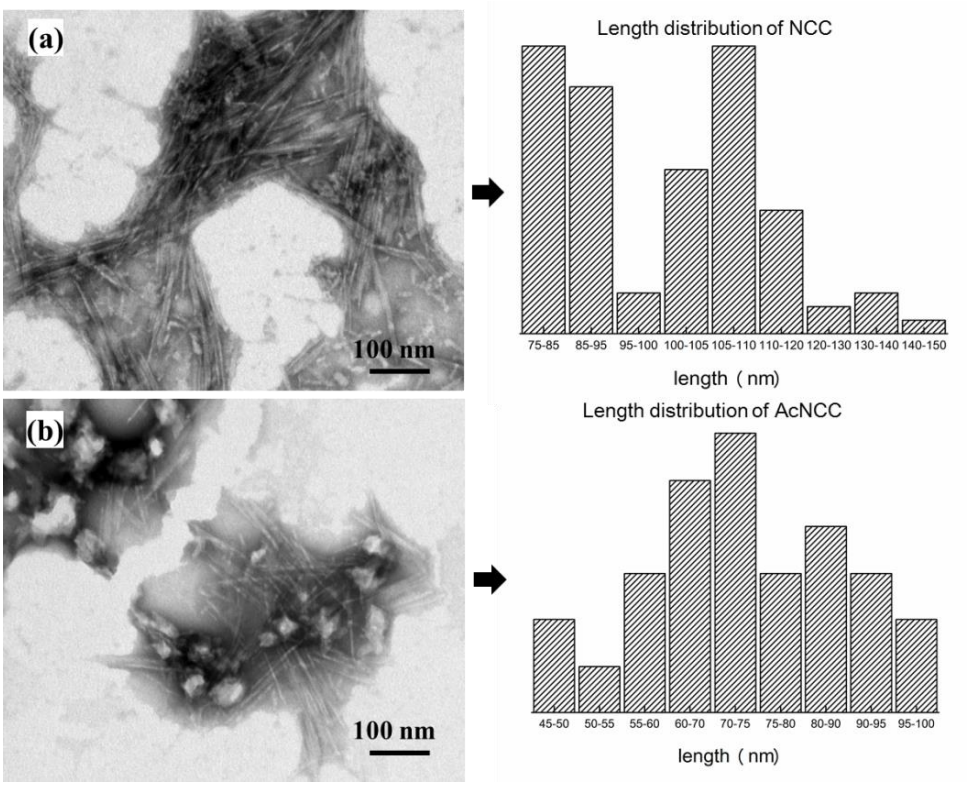

Fig. 1. TEM images and length distribution of the NCC (a) and AcNCC (b)

FT-IR Analysis

Figure 2a shows the infrared spectrum of the NCC. Characteristic peaks for cellulose -OH were observed at 3330 cm^{-1}. This was because the NCC had a broad absorption peak formed from the superposition of multiple -OH stretching vibrational absorption peaks.

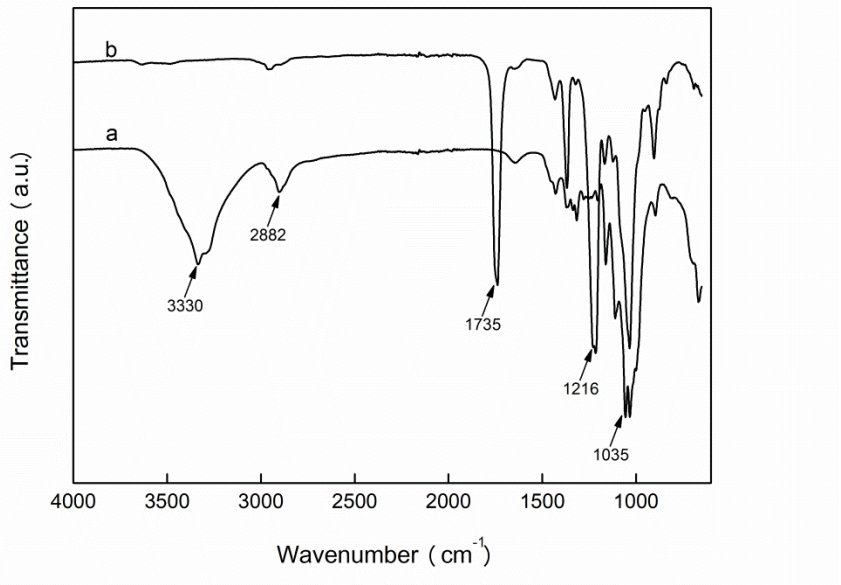

Fig. 2. FT-IR spectra of the NCC (a) and AcNCC (b)

The peak at 2882 cm^{-1} indicated that the corresponding C-H symmetric expansion of the C-H was absorbed by methyl methylene (-CH_2-). Figure 2b shows the infrared spectrum for the AcNCC. An absorption peak for -OH stretching vibration at 3330 cm^{-1} was not present, but a notable C=O stretching vibration absorption peak at 1735 cm^{-1} and characteristic C-O stretching vibration peaks at 1216 cm^{-1} were observed, which indicated that the NCC reacted with acetic anhydride to consume the hydroxyl groups and produced acyl groups. Therefore, AcNCC was successfully prepared through this method.

Figure 3 shows infrared spectra for AcNCC, PLA, and PLA/AcNCC-4 composite film. The adsorption band in the PLA spectrum of Fig. 3 at 1750 cm^{-1} corresponded to a C=O stretching vibration peak. The adsorption bands at 1202 cm^{-1} was a characteristic C-O peak, which illustrated the structural characteristics of the PLA. A comparison of the PLA and PLA/AcNCC-4 spectra indicated that the PLA combined with the AcNCC. The same number of absorption peaks was observed for the composite film and pure PLA because of the low AcNCC content in the composite films. These results showed that the PLA and AcNCC were compatible. There were no other new peaks in the infrared spectrum of the PLA/AcNCC-4 composite membrane, which indicated that the AcNCC and PLA in the composite film were physically combined.

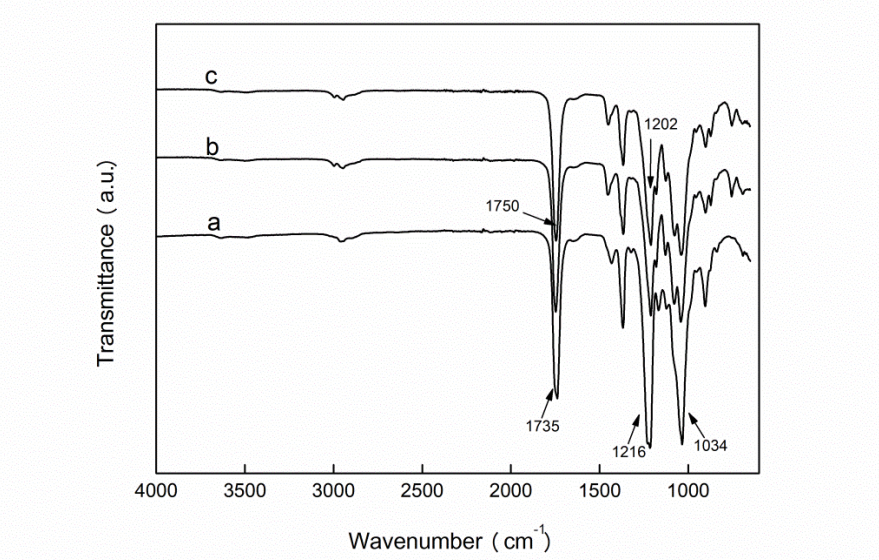

Fig. 3. FT-IR spectra of the AcNCC (a), PLA (b), and PLA/AcNCC-4 (c)

Thermal Properties of the NCC and AcNCC

Figure 4 shows the TGA and differential thermogravimetric (DTG) curves for the NCC and AcNCC. All of the samples showed a small weight loss at temperatures below 110 °C attributable to water evaporation from the materials. Figure 4 shows that the initial degradation temperature of the NCC was 200.9 °C and its maximum thermal degradation temperature was 281.2 °C, which corresponded to the degradation of cellulose. Moreover, the pH of the inner suspension of the NCC was approximately 6. The presence of hydrogen ions (H^+) accelerates dehydration at lower temperatures during pyrolysis (Kim *et al*. 2001; Wang *et al*. 2007). The initial degradation temperature of the AcNCC was 275.6 °C, while its maximum thermal degradation temperature was 356.5 °C. The reason for this may have been because of the decrease in the H^+ content during the acetylation process. These results showed that the thermal stability of the NCC modified by acetylation was considerably improved (Li *et al*. 2011). This thermal stability provides a basis for the application of AcNCC for the enhancement of thermoplastic materials (Spinella *et al*. 2015).

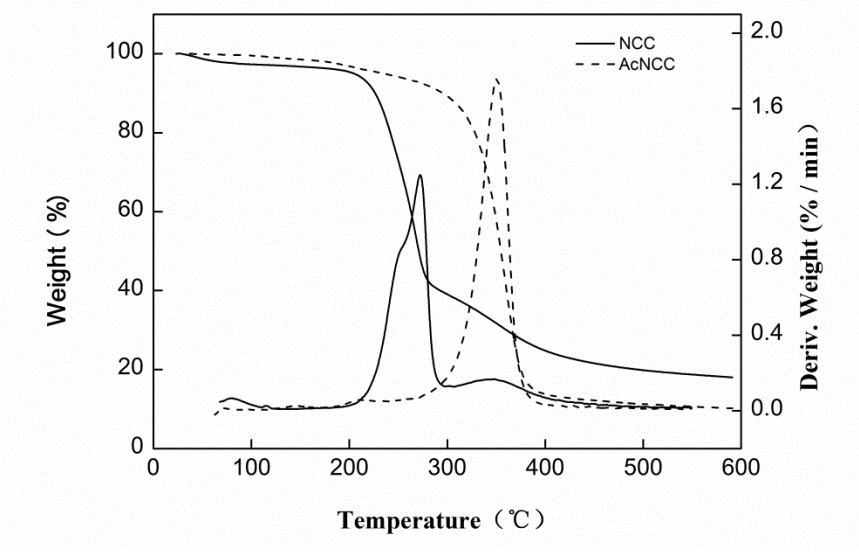

Fig. 4. TGA and DTG curves for the NCC and AcNCC

SEM Analysis of the Composite Films

Figure 5 shows the SEM images of the highly regular porous PLA membranes with different amounts of AcNCC.

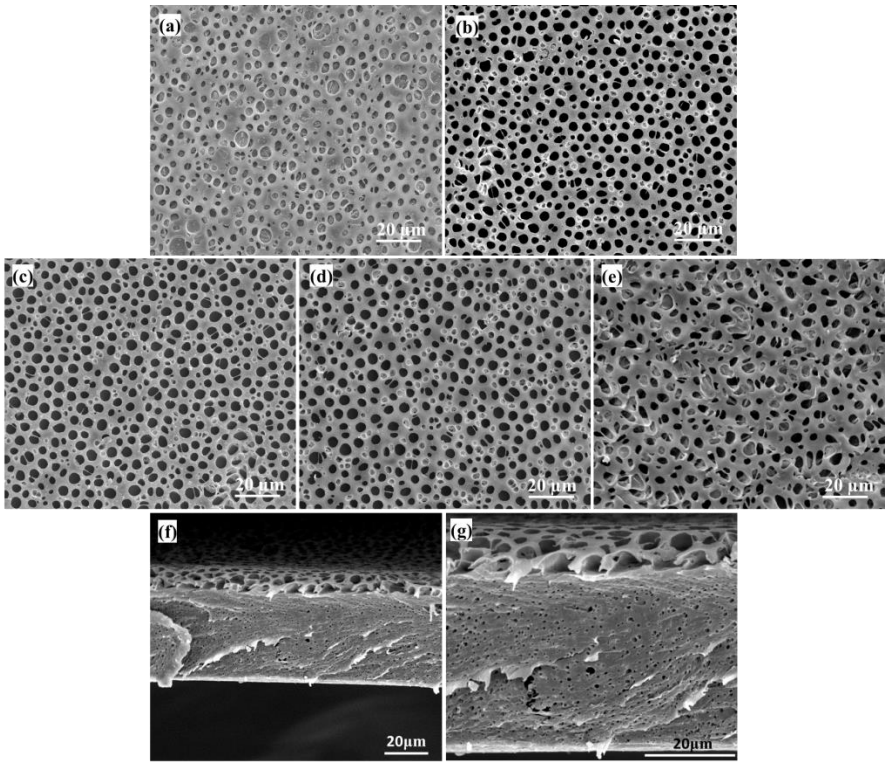

Fig. 5. SEM images of the PLA composites with different AcNCC contents: (a) pure PLA, (b) PLA/AcNCC-2, (c) PLA/AcNCC-4, (d) PLA/AcNCC-8, (e) PLA/AcNCC-12, and (f,g) cross section of PLA/AcNCC-4

The images show that a pore structure was formed in the PLA composite film for all of the AcNCC amounts, but the pore size, distribution, and regularity varied greatly with the AcNCC amount. Figure 5a shows a pure PLA film structure, which had an uneven

pore structure and some of the structure was not formed. As the amount of AcNCC increased, the pore structure became more regular, uniform, and well distributed. The PLA/Ac-NCC-4 showed a uniform pore diameter distribution with diameter of 1.0 μm to 5.0 μm. The cross sectional images of the sample for PLA/Ac-NCC-4 are shown in Figs. 5f and g. The thickness of the film was about 52 μm. Combined with the Figs. 5 a through e, it can be found that the film contain two kinds of pore structures. One is highly regular porous on the surface of the films. The other is the smaller porous structure distribution in the film matrix. When the amount of AcNCC was increased to 12%, the porosity of the composite film decreased. The deformation of the highly regular pore structure may have been because of poor dispersion of the AcNCC in the PLA matrix when the AcNCC concentration was increased.

Mechanical Properties

Figure 6 shows the variation in the tensile strength and Young's modulus of the PLA/AcNCC composite films with different AcNCC contents. The tensile strength and Young's modulus of the composites first increased and then decreased as the AcNCC content was increased. When the AcNCC content was 8%, the tensile strength increased relative to the pure PLA from 19.9 MPa to 41.6 MPa, and the Young's modulus increased relative to the pure PLA from 180.8 MPa to 457.1 MPa. However, as the amount of AcNCC was increased further, the tensile strength and Young's modulus exhibited a decreasing trend.

When the AcNCC content was 12%, the tensile modulus decreased to 26.1 MPa. This could have been because the dispersion of AcNCC in the PLA matrix became poorer as the AcNCC content increased. The aggregation of AcNCC then caused local concentrations of stress and tensile failure occurred prematurely during detection. The tensile strength and Young's modulus of the PLA/AcNCC composites reached maximum values when the AcNCC content was 8%.

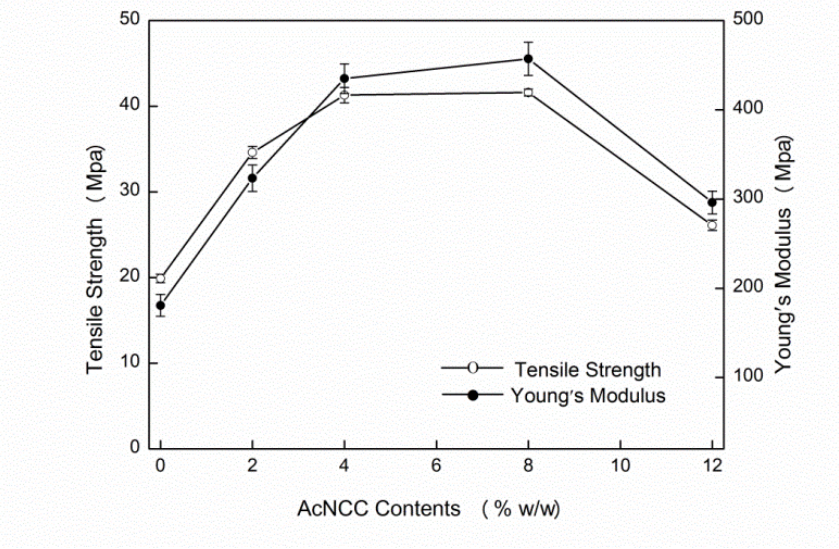

Fig. 6. Mechanical property curves for the PLA/AcNCC composites

Transmittance Analysis

Figure 7 shows a curve for the light transmittance of the PLA/AcNCC composites prepared with different AcNCC amounts. An increase in the AcNCC content caused the light transmittance of the composites to gradually decrease. At an AcNCC content of 8%,

the transmittance decreased drastically from 93% to 60%. The poor dispersion of AcNCC during the preparation process caused the formation of AcNCC nano-filaments in the composite films. The nano-filaments agglomerated into micron- or millimeter-scale fiber bundles, which affected the light transmission. Therefore, an AcNCC content of 4% not only ensured the transparency of the composite material, but also produced a greater enhancement effect, which provided a basis for the application of these composites in the field of high-performance enhanced light-transparent composite materials.

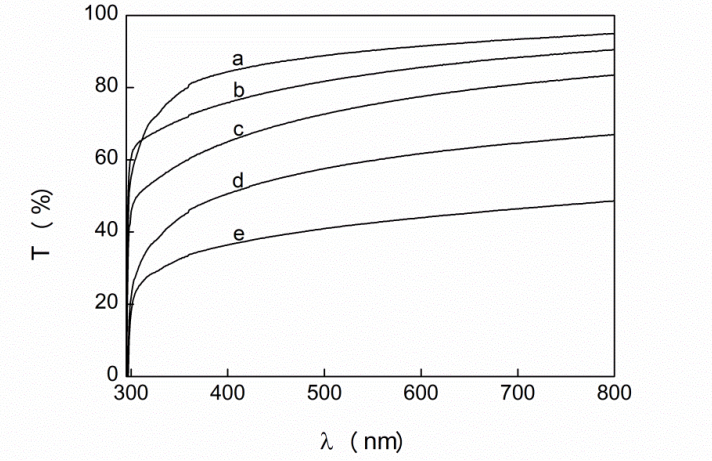

Fig. 7. Transmittance property curves for the PLA/AcNCC composites

TGA of the Composite Films

Figure 8 shows the TGA curves for the PLA/AcNCC composite films with different AcNCC amounts. The DTG curves show that the degradation of the PLA and composite films was divided into two stages at 60 °C to 126 °C and 251.7 °C to 386.2 °C. The TGA curves of the PLA/AcNCC composites showed that the thermal stability of the composites was improved by the addition of AcNCC (Scaffaro *et al*. 2017). The first degradation process in the PLA/AcNCC composites began at a higher temperature than that in the pure PLA. However, the most important result was that the temperature of the second degradation process in the PLA/AcNCC was higher than that of the pure PLA, which indicated an increase in the thermal stability of the PLA/AcNCC.

Combined with the results given in Table 1, the introduction of AcNCC into the PLA resulted in higher maximum decomposition temperatures in the first process (15.4 °C to 25.1 °C) and the maximum decomposition temperatures of the second process increased as well (17.0 °C to 28.9 °C). The latter increase indicated that adding a small portion of AcNCC significantly improved the thermal stability of the PLA/AcNCC. Combined with the mechanical analysis, the results of this study showed that the addition of AcNCC improved the mechanical properties and thermal stability of the PLA/AcNCC composites.

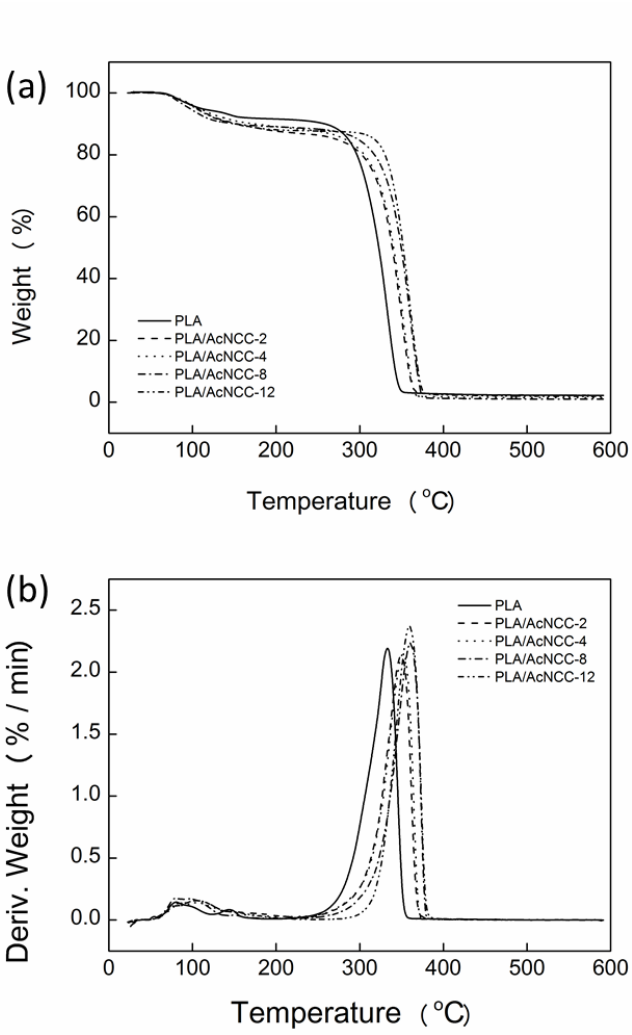

Fig. 8. TGA (a) and DTG curves (b) for the PLA and PLA/AcNCC composites

Table 1. Process Temperatures for the Pure PLA and PLA/AcNCC Composites with Different AcNCC Weight Contents

Sample	First Process	Second Process	
	T_{max} (°C)	Onset Temperature (°C)	T_{max} (°C)
PLA	80.5	245.5	332.9
PLA/AcNCC-2	105.2	250.9	349.9
PLA/AcNCC-4	103.7	248.9	351.7
PLA/AcNCC-8	95.9	258.1	361.8
PLA/AcNCC-12	105.6	253.7	359.2

CONCLUSIONS

1. Porous AcNCC-enhanced PLA highly regular porous composite films with a regular pore structure were prepared with a water-assisted method and used modified AcNCC as an intensifier.

2. The addition of AcNCC improved the mechanical properties and thermal stability of the composite films. The addition of AcNCC also improved the regularity and uniformity of the pore structure.
3. The tensile strength and Young's modulus of the PLA composites were considerably improved at an AcNCC content of 4%, with values that were 2.07 and 2.41 times larger than those of the pure PLA, respectively. The composites also retained an excellent transparency.

ACKNOWLEDGMENTS

This work was financially supported by the National Natural Science Foundation of China (31500467, 31570567), the Natural Science Foundation of Heilongjiang Province for Young Scholars (QC2015034), the Fundamental Research Funds for the Central Universities (2572017CB12), and the Foundation of Key Laboratory of Pulp and Paper Science and Technology of Ministry of Education/Shandong Province of China (KF201708).

REFERENCES CITED

Bilbao-Sáinz, C., Avena-Bustillos, R. J., Wood, D. F., Williams, T. G., and McHugh, T. H. (2010). "Composite edible films based on hydroxypropyl methylcellulose reinforced with microcrystalline cellulose nanoparticles," *J. Agr. Food Chem.* 58(6), 3753-3760. DOI: 10.1021/jf9033128

Fortunati, E., Luzi, F., Puglia, D., Dominici, F., Santulli, C., Kenny, J. M., and Torre, L. (2014). "Investigation of thermo-mechanical, chemical and degradative properties of PLA-limonene films reinforced with cellulose nanocrystals extracted from *Phormium tenax* leaves," *Eur. Polym. J.* 56, 77-91. DOI: 10.1016/j.eurpolymj.2014.03.030

Fortunati, E., Peltzer, M., Armentano, I., Torre, L., Jiménez, A., and Kenny, J. M. (2012). "Effects of modified cellulose nanocrystals on the barrier and migration properties of PLA nano-biocomposites," *Carbohyd. Polym.* 90(2), 948-956. DOI: 10.1016/j.carbpol.2012.06.025

Frone, A. N., Berlioz, S., Chailan, J. F., and Panaitescu, D. M. (2013). "Morphology and thermal properties of PLA–cellulose nanofibers composites," *Carbohyd. Polym.* 91(1), 377-384. DOI: 10.1016/j.carbpol.2012.08.054

Ghalia, M. A., and Dahman, Y. (2017). "Biodegradable poly(lactic acid)-based scaffolds: Synthesis and biomedical applications," *J. Polym. Res.* 24(5), 74-95. DOI: 10.1007/s10965-017-1227-2

Haafiz, M. K. M., Hassan, A., Zakaria, Z., Inuwa, I. M., Islam, M. S., and Jawaid, M. (2013). "Properties of polylactic acid composites reinforced with oil palm biomass microcrystalline cellulose," *Carbohyd. Polym.* 98(1), 139-145. DOI: 10.1016/j.carbpol.2013.05.069

Habibi, Y. (2014). "Key advances in the chemical modification of nanocelluloses," *Chem. Soc. Rev.* 43(5), 1519-1542. DOI: 10.1039/C3CS60204D

Habibi, Y., Lucia, L. A., and Rojas, O. J. (2010). "Cellulose nanocrystals: Chemistry, self-assembly, and applications," *Chem. Rev.* 110(6), 3479-3500.

DOI: 10.1021/cr900339w

Jenekhe, S. A., and Chen, X. L. (1999). "Self-assembly of ordered microporous materials from rod-coil block copolymers," *Science* 283, 372-375. DOI: 10.1126/science.283.5400.372

Kim, D.-Y., Nishiyama, Y., Wada, M., and Kuga, S. (2001). "High-yield carbonization of cellulose by sulfuric acid impregnation," *Cellulose* 8(1), 29-33. DOI: 10.1023/A:1016621103245

Kowalczyk, M., Piorkowska, E., Kulpinski, P., and Pracella, M. (2011). "Mechanical and thermal properties of PLA composites with cellulose nanofibers and standard size fibers," *Compos. Part A-Appl. S.* 42(10), 1509-1514. DOI: 10.1016/j.compositesa.2011.07.003

Lam, N. T., Saewong, W., and Sukyai, P. (2017). "Effect of varying hydrolysis time on extraction of spherical bacterial cellulose nanocrystals as a reinforcing agent for poly(vinyl alcohol) composites," *J. Polym. Res.* 24(5), 71-81. DOI: 10.1007/s10965-017-1232-5

Li, W., Wang, R., and Liu, S. (2011). "Nanocrystalline cellulose prepared from softwood kraft pulp *via* ultrasonic-assisted acid hydrolysis," *BioResources* 6(4), 4271-4281. DOI: 10.15376/biores.6.4.4271-4281

Li, W., Zhao, X., Huang, Z., and Liu, S. (2013a). "Nanocellulose fibrils isolated from BHKP using ultrasonication and their reinforcing properties in transparent poly (vinyl alcohol) films," *J. Polym. Res.* 20(8), 210-216. DOI: 10.1007/s10965-013-0210-9

Li, W., Zhao, X., and Liu, S. (2013b). "Preparation of entangled nanocellulose fibers from APMP and its magnetic functional property as matrix," *Carbohyd. Polym.* 94(1), 278-285. DOI: 10.1016/j.carbpol.2013.01.052

Lin, N., Huang, J., Chang, P. R., Feng, J., and Yu, J. (2011). "Surface acetylation of cellulose nanocrystal and its reinforcing function in poly(lactic acid)," *Carbohyd. Polym.* 83(4), 1834-1842. DOI: 10.1016/j.carbpol.2010.10.047

Nakagaito, A. N., Fujimura, A., Sakai, T., Hama, Y., and Yano, H. (2009). "Production of microfibrillated cellulose (MFC)-reinforced polylactic acid (PLA) nanocomposites from sheets obtained by a papermaking-like process," *Compos. Sci. Technol.* 69(7-8), 1293-1297. DOI: 10.1016/j.compscitech.2009.03.004

Pankaj, S. K., Bueno-Ferrer, C., Misra, N. N., O'Neill, L., Jiménez, A., Bourke, P., and Cullen, P. J. (2014). "Characterization of polylactic acid films for food packaging as affected by dielectric barrier discharge atmospheric plasma," *Innov. Food Sci. Emerg.* 21, 107-113. DOI: 10.1016/j.ifset.2013.10.007

Robles, E., Urruzola, I., Labidi, J., and Serrano, L. (2015). "Surface-modified nano-cellulose as reinforcement in poly(lactic acid) to conform new composites," *Ind. Crop. Prod.* 71, 44-53. DOI: 10.1016/j.indcrop.2015.03.075

Scaffaro, R., Botta, L., Lopresti, F., Maio, A., and Sutera, F. (2017). "Polysaccharide nanocrystals as fillers for PLA based nanocomposites," *Cellulose* 24(2), 447-478. DOI: 10.1007/s10570-016-1143-3

Shi, Q., Zhou, C., Yue, Y., Guo, W., Wu, Y., and Wu, Q. (2012). "Mechanical properties and *in vitro* degradation of electrospun bio-nanocomposite mats from PLA and cellulose nanocrystals," *Carbohyd. Polym.* 90(1), 301-308. DOI: 10.1016/j.carbpol.2012.05.042

Shimomura, M. (1993). "Preparation of ultrathin polymer films based on two-dimensional molecular ordering," *Prog. Polym. Sci.* 18(2), 295-339. DOI: 10.1016/0079-6700(93)90028-B

Spinella, S., Re, G. L., Liu, B., Dorgan, J., Habibi, Y., Leclère, P., Raquez, J.-M., Dubois, P., and Gross, R. A (2015). "Polylactide/cellulose nanocrystal nanocomposites: Efficient routes for nanofiber modification and effects of nanofiber chemistry on PLA reinforcement," *Polymer* 65, 9-17. DOI: 10.1016/j.polymer.2015.02.048

Srinivasarao, M., Collings, D., Philips, A., and Patel, S. (2001). "Three-dimensionally ordered array of air bubbles in a polymer film," *Science* 292, 79-83. DOI: 10.1126/science.1057887

Wang, N., Ding, E., and Cheng, R. (2007). "Thermal degradation behaviors of spherical cellulose nanocrystals with sulfate groups," *Polymer* 48(12), 3486-3493. DOI: 10.1016/j.polymer.2007.03.062

Widawski, G., Rawiso, M., and François, B. (1994). "Self-organized honeycomb morphology of star-polymer polystyrene films," *Nature* 369(6479), 387-389. DOI: 10.1038/369387a0

Xie, L., Xu, H., Wang, Z.-P., Li, X.-J., Chen, J.-B., Zhang, Z.-J., Yin, H.-M., Zhong, G.-J., Lei, J., and Li, Z.-M. (2014). "Toward faster degradation for natural fiber reinforced poly(lactic acid) biocomposites by enhancing the hydrolysis-induced surface erosion," *J. Polym. Res.* 21(3), 357-371. DOI: 10.1007/s10965-014-0357-z

Zhao, X., Cai, Q., Shi, G., Shi, Y., and Chen, G. (2003). "Formation of ordered microporous films with water as templates from Poly (D,L-lactic-*co*-glycolic acid) solution," *J Appl. Polym. Sci*. 90, 1846-1850. DOI: 10.1002/app.12836

Article submitted: June 27, 2018; Peer review completed: August 31, 2018; Revised version received: September 9, 2018; Accepted: September 10, 2018; Published: September 26, 2018.
DOI: 10.15376/biores.13.4.8432-8443